Testing the impact of clouds on the radiation budgets of 19 atmospheric general circulation models

Gerald L. Potter

Program for Climate Model Diagnosis and Intercomparison, Lawrence Livermore National Laboratory, Livermore, California, USA

Robert D. Cess

Marine Sciences Research Center, State University of New York at Stony Brook, Stony Brook, New York, USA

Received 28 July 2003; revised 4 November 2003; accepted 13 November 2003; published 27 January 2004.

[1] We compare cloud-radiative forcing (CRF) at the top-of-the atmosphere from 19 atmospheric general circulation models, employing simulations with prescribed sea-surface temperatures, to observations from the Earth Radiation Budget Experiment (ERBE). With respect to 60°N to 60°S means, a surprising result is that many of the 19 models produce unusually large biases in Net CRF that are all of the same sign (negative), meaning that many of the models significantly overestimate cloud radiative cooling. The primary focus of this study, however, is to demonstrate a diagnostic procedure, using ERBE data, to test if a model might produce, for a given region, reasonable CRF as a consequence of compensating errors caused either by unrealistic cloud vertical structure, cloud optical depth or cloud fraction. For this purpose we have chosen two regions, one in the western tropical Pacific characterized by high clouds spanning the range from thin cirrus to deep convective clouds, and the other in the southeastern Pacific characterized by trade cumulus. For a subset of eight models, it is found that most typically produce more realistic regionally-averaged CRF (and its longwave and shortwave components) for the southeastern region as opposed to the western region. However, when the diagnostic procedure for investigating cloud vertical structure and cloud optical depth is imposed, this somewhat better agreement in the southeastern region is found to be the result of compensating errors in either cloud vertical structure, cloud optical depth or cloud fraction. The comparison with ERBE data also shows large errors in clear-sky fluxes for many of the models. *INDEX TERMS:* 1620 Global Change: Climate dynamics (3309); 1610 Global Change: Atmosphere (0315, 0325); 3359 Meteorology and Atmospheric Dynamics: Radiative processes; 3309 Meteorology and Atmospheric Dynamics: Climatology (1620); *KEYWORDS:* radiation, climate, clouds

Citation: Potter, G. L., and R. D. Cess (2004), Testing the impact of clouds on the radiation budgets of 19 atmospheric general circulation models, *J. Geophys. Res.*, *109*, D02106, doi:10.1029/2003JD004018.

1. Introduction

[2] Cloud-climate interactions comprise one of the greatest uncertainties in attempting to model climate change using general circulation models (GCMs), and there is a need to devise ways of testing such interactions within models. As *Webb et al.* [2001] emphasize: "If we are to have confidence in predictions from climate models, a necessary (although not sufficient) requirement is that they should be able to reproduce the observed present-day distribution of clouds and their associated radiative fluxes." Since the availability of the Earth Radiation Budget Experiment (ERBE) data [*Ramanathan et al.*, 1989; *Harrison et al.*, 1990], there have been numerous comparisons of models to the ERBE top-of-the-atmosphere (TOA) radiative fluxes. For example, a comparison of seasonal changes of cloud-radiative forcing (CRF), as produced by 18 GCMs, to ERBE satellite data showed substantial differences, and more importantly provided clues as to the deficiencies of some models [*Cess et al.*, 1997]. In their study, *Webb et al.* [2001] added an additional constraint by combining ERBE data with cloud-top pressures determined by the International Satellite Cloud Climatology Project (ISCCP) [*Rossow and Schiffer*, 1991]. Such a combined test is important, because as we later emphasize, it is possible for a model to produce, for a given region, reasonable TOA CRF as a consequence of compensating errors caused either by unrealistic cloud vertical structure, cloud optical depth or cloud fraction.

[3] In the present study we adopt the procedure used by *Cess et al.* [2001a, 2001b], who studied cloud vertical structure anomalies over the tropical Pacific during the strong 1997/1998 El Niño. This involved interfacing shortwave (SW) and longwave (LW) CRF, as measured both by ERBE and the Clouds and the Earth's Radiant Energy

0148-0227/04/2003JD004018$09.00

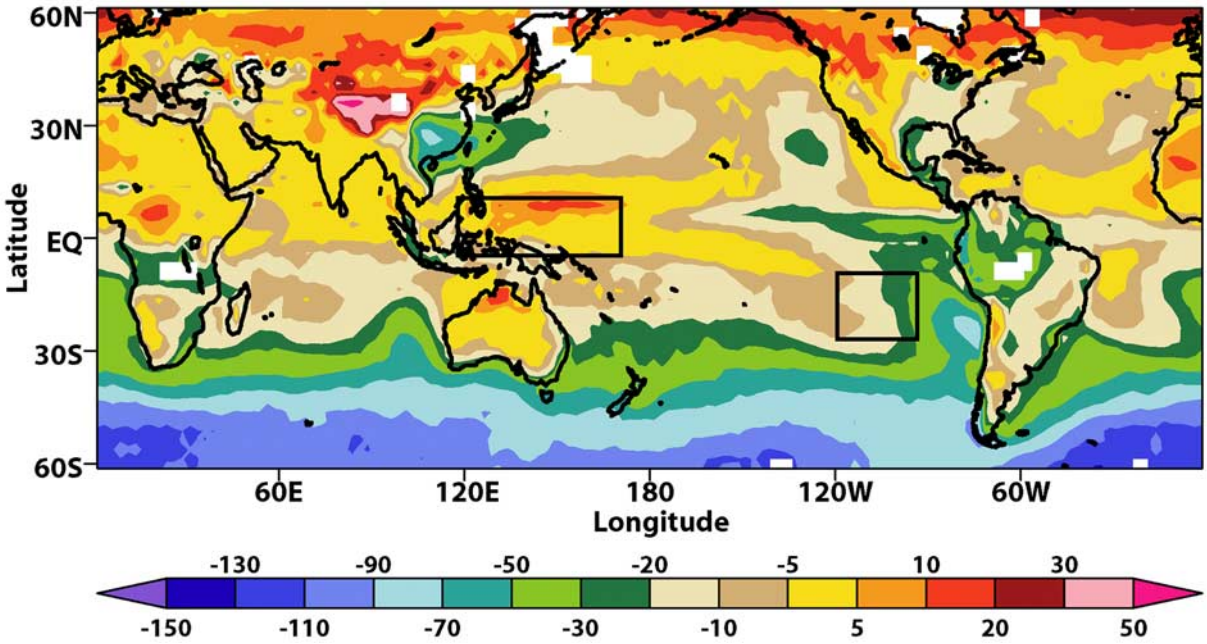

Figure 1. The geographical distribution of Net CRF from the ERBE data for DJF and averaged over the five ERBE years (1985–1989). The western and southeastern Pacific study regions are outlined in black.

System (CERES), so as to infer changes in cloud vertical structure. These changes were in turn shown to be consistent with measurements of the vertical distribution of clouds based on observations by the Stratospheric Aerosol and Gas Experiment (SAGE) II [*Cess et al.*, 2001b]. In the present study we employ five years of ERBE data (1985–1989) to determine both CRF and cloud vertical structure for two regions of the Pacific, a tropical western region characterized by high clouds and a southeastern region characterized by trade cumulus. For these two study regions, this data set is used to test the impact of clouds on the radiation budgets of 19 atmospheric GCMs for the same time period as the ERBE data. Although there have been numerous comparisons of GCMs to ERBE data, this study additionally addresses the issue of how well the models depict cloud vertical structure and cloud optical depth for the 1985–1989 period.

2. Earth Radiation Budget Experiment (ERBE) Data

[4] The ERBE data consist of the monthly-mean CRF measurements on 2.5° × 2.5° grids and for the 5-year ERBE period (1985–1989) [*Harrison et al.*, 1990]. The SW and LW components of CRF [*Ramanathan et al.*, 1989; *Harrison et al.*, 1990] are defined as

$$\mathrm{SWCRF} = \mathrm{R_C} - \mathrm{R}$$

where R denotes the TOA all-sky reflected SW and $\mathrm{R_C}$ that for clear skies, while

$$\mathrm{LWCRF} = \mathrm{F_C} - \mathrm{F}$$

where *F* and $\mathrm{F_C}$, respectively, denote the all-sky and clear-sky TOA emitted LW. Typically SW CRF is negative (cooling) and LW CRF positive (heating). The Net CRF is simply the sum of the components

$$\text{Net CRF} = \text{SW CRF} + \text{LW CRF}$$

and cancellation between SW CRF cooling and LW CRF heating (Net CRF = 0) can be expressed by the ratio

$$\mathrm{N} = -(\text{SW CRF})/(\text{LW CRF}) = 1$$

If N > 1, SW cooling dominates, whereas LW heating dominates for N < 1.

[5] Figure 1 shows the geographical distribution of the Net CRF for the DJF period and averaged over the five ERBE years (1985–1989). The western and southeastern study regions are outlined in black, and the boundaries of the two regions are 10.0°N to 5.0°S and 117.5°E to 170.0°E for the western region, and 10.0°S to 27.5°S and 92.5°W to 120.0°W for the southeastern region. As is well known [*Kiehl and Ramanathan*, 1990; *Kiehl*, 1994; *Hartmann et al.*, 2001], there is near cancellation between the LW and SW components of CRF (Net CRF ≈ 0, N ≈ 1) in regions of deep convection such as the western study region. The trade cumulus clouds of the southeastern region, however, have lower cloud-top altitudes and hence, relative to SW CRF, smaller LW CRF because the cloud are warmer, so SW cooling dominates.

[6] Shown in Figure 2a is a scatterplot of ERBE LW CRF versus SW CRF for the two study regions. Each point represents a DJF mean averaged over the five ERBE years (1985 to 1989), and for each 2.5° × 2.5° ERBE grid within the respective regions. Thus the number of points corresponds to the number of ERBE grids within each region (126 for the western region and 96 for the southeastern region). Because the data constitute 15-month means, the points in Figure 2a cannot be taken as representative of

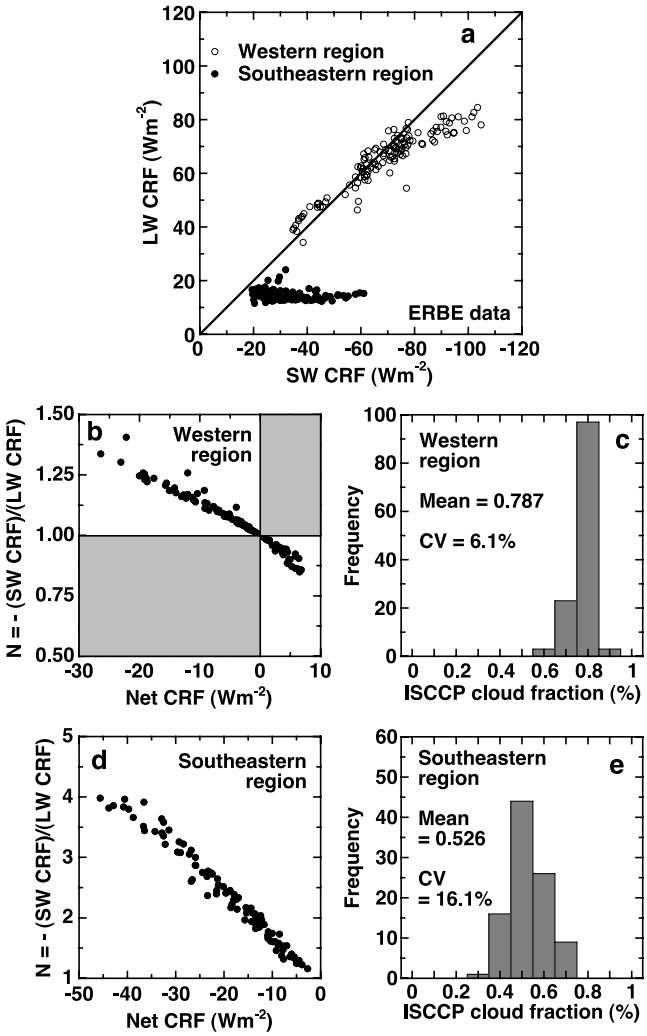

Figure 2. (a) Scatterplot LW CRF versus SW CRF for the two study regions. Each point represents a DJF mean averaged over the five ERBE years (1985 to 1989) and for each 2.5° × 2.5° ERBE grid within each region. (b) Scatterplot of N versus Net CRF for the ERBE data in the western study region. The shaded quadrants represent domains that are not physically possible. (c) Frequency distribution of ISCCP cloud fraction for the western study region. The coefficient of variation (CV) is the standard deviation as a percentage of the mean. (d) The same as (b) but for the southeastern study region and for only the upper left-hand quadrant, which for the southeastern region is the only quadrant within which the data lie. (e) The same as (c) but for the southeastern study region.

unique cloud systems. However, they should be representative, at least to first order, as time-averages of cloud systems that are dominant in a specific region, such as cirrus in the western region and trade cumulus in the southeastern region. In this context, for the western region the near-cancellation between the LW and SW components of CRF [*Kiehl and Ramanathan*, 1990; *Kiehl*, 1994; *Hartmann et al.*, 2001] is evidenced by the close proximity of the data points to the 45° diagonal line. When averaged over the western region, SW CRF = -69.0 Wm^{-2}, LW CRF = 65.0 Wm^{-2}, and N = 1.06. Since LW and SW CRF are both linearly proportional to cloud fraction [*Kiehl*, 1994; *Cess et al.*, 2001a], the progression of the data points from left to right could be attributed to an increase in cloud fraction, or to an increase in cloud optical depth which would simultaneously increase cloud albedo (increase SW CRF) and cloud emissivity (increase LW CRF), or to a combination of the two. For the southwestern region, on the other hand, the progression of the data points from left to right shows minimal change in LW CRF, despite the increase in SW CRF. One possible explanation is that these thicker lower-level clouds, relative to the western region, are black in the infrared (cloud emissivity = 1) and exhibit little change in cloud-top altitude (cloud-top temperature) throughout the region. Thus an increase in cloud optical depth would increase SW CRF but not LW CRF. In addition, since LW CRF is linearly proportional to cloud fraction, the near constancy of LW CRF could imply that cloud fraction is spatially uniform over the southeastern region. Further discussion on these points will be provided shortly.

[7] *Cess et al.* [2001a, 2001b] employed scatterplots of N versus Net CRF as a diagnostic of changes in tropical cloud vertical structure associated with the 1997/98 El Niño, and in the present study we adopt, for the two study regions, these plots as a means of testing GCMs. The N versus Net CRF scatterplot is shown in Figure 2b for the western region. *Cess et al.* employed an atmospheric radiation model as an aid to interpreting such scatterplots, and for Figure 2b their explanation is as follows. The shaded quadrants represent domains that are not physically possible, whereas the lower right-hand quadrant denotes net heating and the upper left-hand quadrant net cooling. As cloud optical depth is increased from an initial value of zero (clear skies, Net CRF = 0, N = 1), both cloud emissivity and albedo increase, but with the former dominating so that Net CRF increases (warming). This reverses when the albedo increases more rapidly than the emissivity (the emissivity ultimately asymptotes to unity), and so the left-to-right progression reverses and returns to the Net CRF = 0 and N = 1 intercept (which in this case represents SW/LW cloud compensation as opposed to clear skies). A further increase in cloud optical depth then results in a progression into the cooling quadrant.

[8] Since N is invariant to cloud fraction while Net CRF is linearly proportional to cloud fraction [*Kiehl*, 1994; *Cess et al.*, 2001a], a reduction of cloud fraction would produce a horizontal progression of points with Net CRF going to zero as cloud fraction tends to zero. Thus in terms of data, horizontal scatter would correspond to variations in cloud fraction, whereas vertical scatter would imply variations in cloud altitude, since a decrease in cloud altitude would reduce LW CRF and thus increase N. The lack of such scatter in Figure 2b could imply spatial uniformity of both cloud fraction and cloud altitude within the context of 15-month means. Data from the International Satellite Cloud Climatology Project (ISCCP) are in fact consistent with a nearly spatial uniformity of cloud fraction over the western region. This is demonstrated by the frequency distribution shown in Figure 2c, for which the ISCCP data correspond to the same 15-month means and 2.5° × 2.5° grids as the ERBE data. Thus at least to first order, variations in cloud fraction do not appear to be a cause for the Net CRF variation shown in

Table 1. Summary of the 19 Atmospheric General Circulation Models

Acronym	Group	Location
BMRC	Bureau of Meteorology Research Center	Melbourne, Australia
CCCMA	Canadian Centre for Climate Modeling and Analysis	Victoria, Canada
CCSR	Center for Climate System Research	Tokyo, Japan
CNRM	Centre Natianal de Recherches Meteorologiques	Toulouse, France
COLA	Center for Ocean-Land-Atmospheres Studies	Calverton, Maryland
ECMWF	European Centre for Medium-Range Weather Forecasts	Reading, UK
GFDL	Geophysical Fluid Dynamics Laboratory	Princeton, New Jersey
GISS	Goddard Institute for Space Studies	New York, New York
GLA	Goddard Laboratory for Atmospheres	Greenbelt, Maryland
JMA	Japan Meteorological Agency	Tokyo, Japan
MGO	Main Geophysical Observatory	St. Petersburg, Russia
MPI	Max-Planck-Institut fur Meteorologie	Hamburg, Germany
MRI	Meteorological Research Institute	Ibaraki-ken, Japan
NCAR	National Center for Atmospheric Research	Boulder, Colorado
NCEP	National Centers for Environmental Prediction	Suitland, Maryland
SUNYA	State University of New York at Albany	Albany, New York
UGAMP	The UK Universities' Global Atmospheric Modeling Programme	Reading, UK
UIUC	University of Illinois at Urbana-Champaign	Urbana, Illinois
UKMO	United Kingdom Meteorological Office	Exeter, UK

Figure 2b, nor for the SW CRF and LW CRF variation in Figure 2a for the western region. Although one anticipates, for temporal averages, a negative correlation between cloud optical depth (i.e., cloud liquid water path) and cloud-top altitude [*Hack*, 1998; *Zhou and Cess*, 2001], it is difficult to conceive that this would contribute to the lack of scatter in Figure 2b. To put it another way, it is improbable that if there were spatial variations in cloud-top altitude, which by itself would cause vertical scatter in Figure 2b, that corresponding changes in cloud optical depth would minimize this scatter. For example, as an illustration consider a decrease in average cloud-top altitude for one of the points in the cooling (upper left-hand) quadrant of Figure 2b. This by itself would decrease LW CRF and increase N, thus moving the point vertically upward. The related decrease in Net CRF would move the point slightly to the right (the slope of a linear regression to the data is -0.015). Next, if we allow cloud optical depth to increase as the result of the reduction in cloud-top altitude, this by itself would further increase N through the increase in SW CRF, while there would be only a slight shift to the left, from the already shifted position to the right, due to the related decrease in Net CRF. The net effect would be a departure of the data point from the tight ensemble formed by the other data points. Thus the lack of scatter in Figure 2b appears to be the result of a lack of spatial variability of both cloud fraction and cloud-top altitude within the western region, with the variation in N and Net CRF being driven by changes in cloud optical depth which also cause the changes in LW CRF and SW CRF shown in Figure 2a.

[9] The ERBE N versus Net CRF scatterplot is shown in Figure 2d for the southeastern region, and note the different vertical scales in Figures 2b and 2d, consistent with the cloud-top altitudes being lower in the southeastern region (larger N) relative to the western region. Like Figure 2b, there is minimal scatter of the data points in Figure 2d. As discussed with reference to Figure 2a, the near constancy of LW CRF suggests a lack of spatial variability of cloud-top altitude within the southeastern region. However, unlike the western region, the ISCCP data suggest moderate spatial variability of cloud fraction (Figure 2e). Thus the lack of scatter in Figure 2d does not have as straightforward an explanation as for the western region (Figure 2b). However, the cloud variability shown in Figure 2e is consistent with the modest vertical scatter of LW CRF in Figure 2a, since CV = 13.8% for the former and 16.1% for the latter, and recall that LW CRF is linearly proportional to cloud fraction.

[10] We reiterate the point made earlier that the data shown in Figure 2 constitute 15-month means and thus cannot be taken as representative of unique cloud systems. Nor should these 15-month means be construed as representing a single cloud type. That cloud altitudes and cloud fractions, averaged over the 15-month period, seem to exhibit only modest geographical variability for both study regions certainly does not imply that every cloudy day has the same cloud altitude and cloud fraction during the 15-month period.

3. General Circulation Model/ERBE Comparisons

[11] The atmospheric GCMs used in the present study are summarized in Table 1, and the simulations are from the Atmospheric Model Intercomparison Project (AMIP) II (see *Gates et al.* [1999] for a description of AMIP I) in which the models are run with prescribed sea-surface temperatures (SSTs). To facilitate comparison with the ERBE data, the GCM's SW and LW CRF were interpolated to the ERBE $2.5^\circ \times 2.5^\circ$ grids using a linear area-weighted interpolation. However, before proceeding with the N versus Net CRF scatterplot comparisons, it is instructive to compare the models to the ERBE zonal-mean Net CRF as well as its SW and LW components. These comparisons are shown in Figure 3, with the restriction to 60°N to 60°S since the ERBE clear-sky scene identification is not reliable over snow and ice [*Nemesure et al.*, 1994]. What is revealing is that, as shown in Figure 3a, and with the exception of high latitudes, the models either agree with the ERBE Net CRF or produce a negative bias. Also, as demonstrated in Figures 3b and 3c, this bias is primarily associated with the SW CRF. The same point is made when considering 60°N to 60°S means as demonstrated in Figures 4a and 4b. Here and in the following, bias is defined as the difference

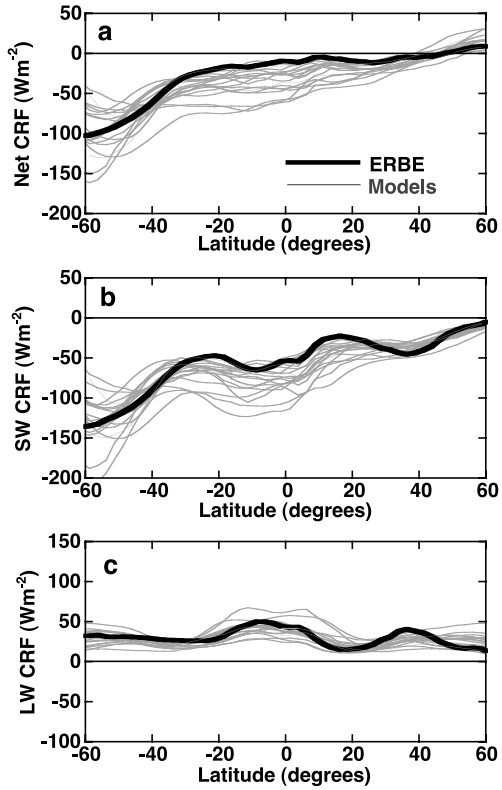

Figure 3. (a) Zonal mean Net CRF for the 19 GCMs compared with that for ERBE. These are for DJF and averaged over the five ERBE years (1985–1989). (b) The same as (a) but for SW CRF. (c) The same as (a) but for LW CRF.

between the model relative to ERBE. It is important to emphasize that the AMIP runs specify the SST as a boundary condition, such that the atmospheric models do not have to be in radiative balance at the TOA; energy can be created or destroyed at the ocean surface without any requirement for balance. However, the degree of imbalance does not explain the Net CRF biases in Figure 4a. The imbalance for each model is shown in Figure 4c as the annually and globally averaged net downward radiative flux at the TOA which, for radiative balance, would be zero. There is no significant correlation between the results shown in Figures 4a and 4c.

[12] Admittedly, the agreement of some models with ERBE may be the result of their being tuned to the ERBE CRF. However, the fact remains that many models produce significant biases, and it is not the intent of this study to understand the causes of the larger biases. Rather, the intent is to examine whether those models that produce minimal or modest biases in Figure 4 are doing so for the right reasons or, alternatively, if they are doing so as the result of compensating errors. For this reason, we restrict attention to a subset of models for which the CRF biases are summarized in Figure 5 for the two study regions. Our exclusion of SUNYA is because the results for this model are very similar to NCAR from which SUNYA was derived.

[13] We now proceed to comparing model outputs to the ERBE data shown in the N versus Net CRF scatterplots of Figures 2b and 2d. In selecting the two study regions, care

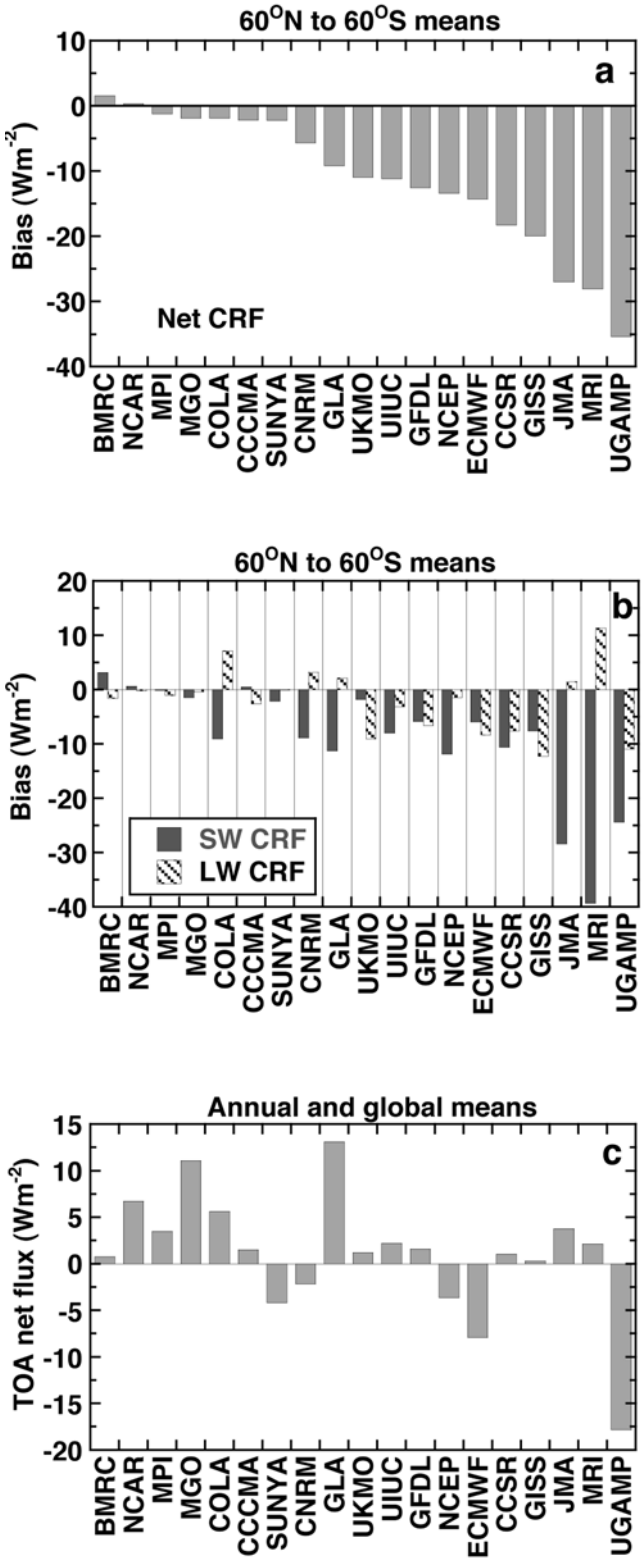

Figure 4. (a) The Net CRF biases, relative to ERBE and averaged from 60°S to 60°N, for each of the 19 GCMs. (b) The same as (a) but for SW and LW CRF biases. (c) The net downward TOA radiative flux, globally averaged, for the 19 GCMs.

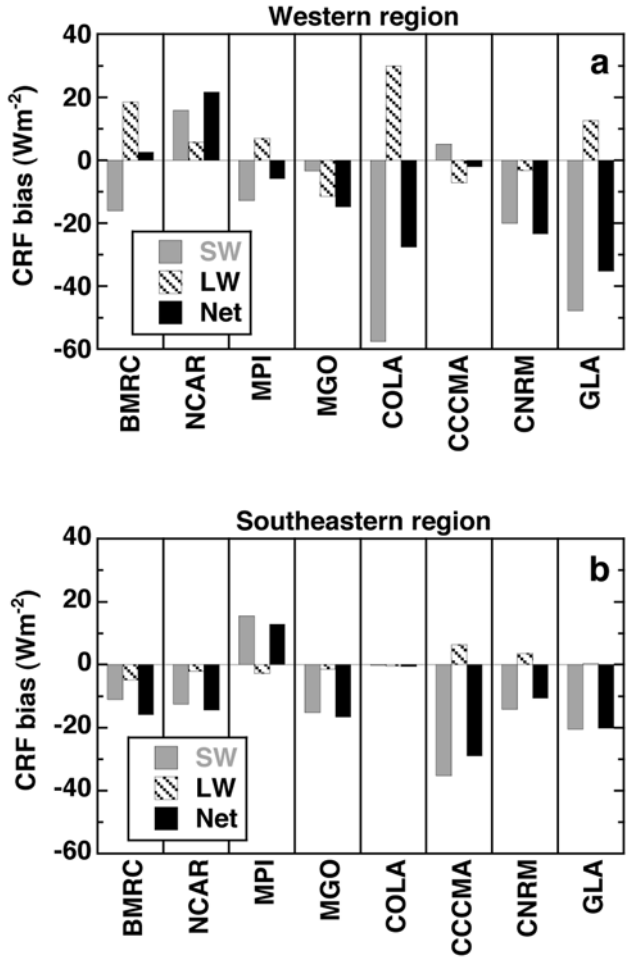

Figure 5. (a) The SW, LW and Net CRF biases, relative to ERBE, for each of the eight selected GCMs and averaged over the western study region. (b) The same as (a) but for the southeastern study region.

was exercised to assure that none of the eight models produced a change from one cloud system to another within the respective study region. That is, to assure that a model's errors, relative to ERBE, were not the result of the model producing realistic clouds, but placing those clouds in the wrong location. This was accomplished by varying the boundaries of each region until N versus Net CRF scatterplots were obtained for each region, and for each model, that were essentially independent of the region's boundaries.

[14] The N versus Net CRF scatterplots for the eight selected models are summarized in Figure 6 for the western region and compared to the ERBE data shown in Figure 2b. Both BMRC and NCAR do a laudable job of replicating ERBE with but one exception, they both produce excessive thin cirrus clouds as evidenced by the model points extending beyond the ERBE points in the lower right-hand quadrant. These are the only two models that produce a positive Net CRF bias for the western region (Figure 5a), although modest for BMRC, and this is partially caused by the excessive thin cirrus. CCCMA likewise produces some excessive thin cirrus, but there is a population of overly bright (thick) clouds to the left of the ERBE points that offsets this, with the result that the overly thin and thick clouds compensate each other and produce the minimal biases shown in Figure 5a. In other words, this model produces too broad a distribution of cloud optical depths, with the smaller and larger optical depths essentially compensating each other. CNRM also produces overly bright clouds, but without compensatory thin clouds, so that there is a negative SW CRF bias (Figure 5a). This is also the case for both COLA and GLA, which have the largest SW CRF biases in Figure 5a. These models also produce an interesting nonlinear behavior, possibly caused by a systematic increase in cloud-top altitude with increasing cloud optical depth. With the exception of a small lack of thin cirrus clouds, MPI does a good job of replicating ERBE, consis-

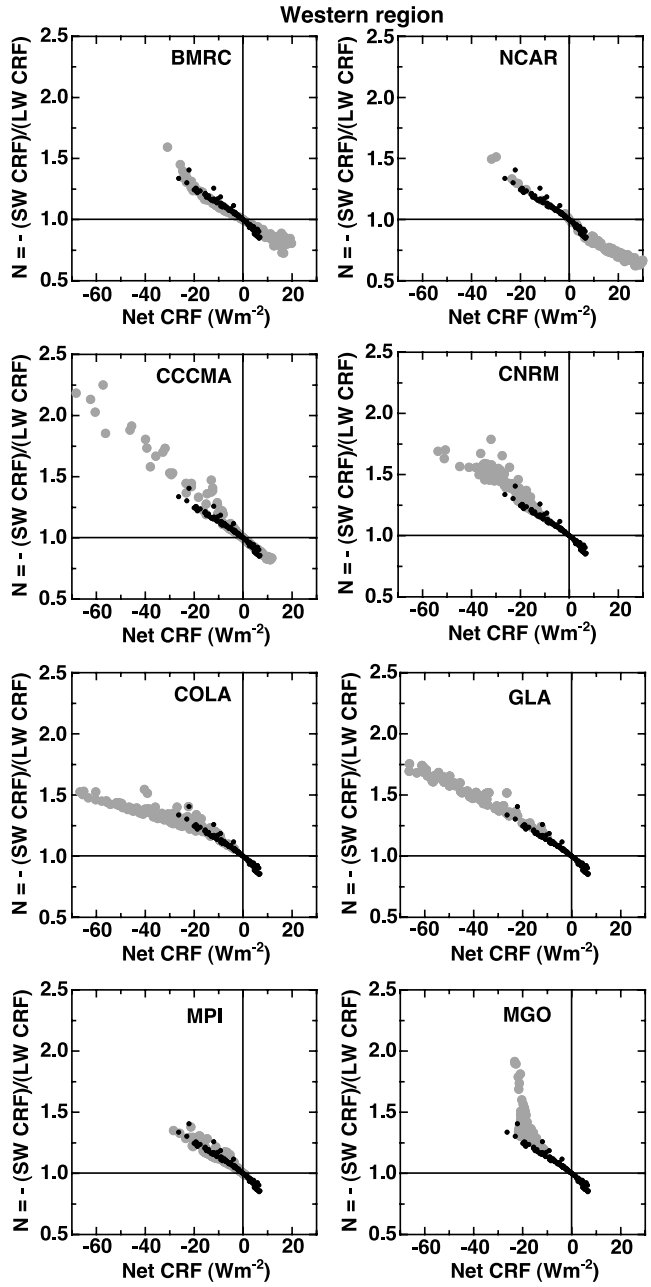

Figure 6. The same as Figure 2b, but for the eight selected GCMs as denoted by the gray filled circles. The black dots represent the ERBE data from Figure 2b.

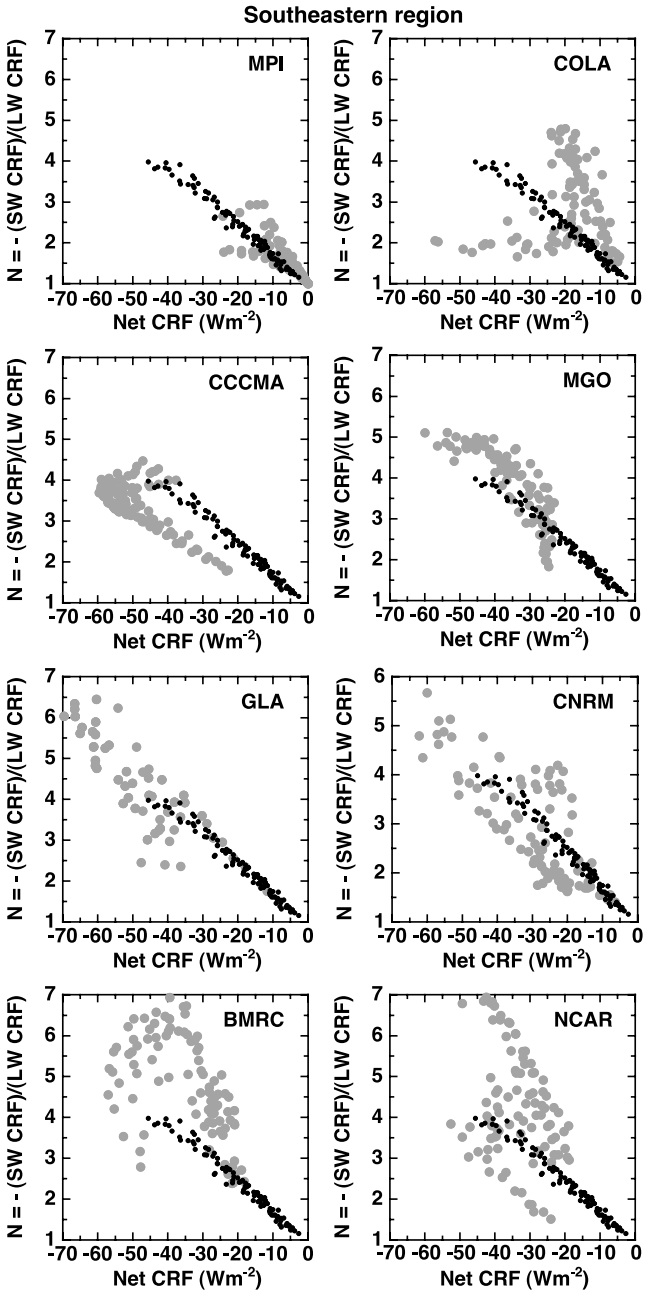

Figure 7. The same as Figure 2d, but for the eight selected GCMs as denoted by the gray filled circles. The black dots represent the ERBE data from Figure 2d.

tent with the minimal biases shown in Figure 5a. MGO is interesting, since the spatially averaged biases in Figure 5a are modest, yet this model differs significantly in Figure 6 from the ERBE points. That the model's points show extreme vertical scatter suggests, unlike the inference from the ERBE data, that the model's cloud-top altitudes exhibit substantial variability over the domain of the western region, while the regional mean biases in CRF are small (Figure 5a). For this model, agreement with the observed radiative fluxes is achieved through compensating errors in cloud fraction, vertical structure, and cloud optical properties.

[15] Figure 7 provides a similar summary as Figure 6, but for the southeastern region. The ability of the models to replicate the ERBE data, in the context of the N versus Net CRF scatterplots, is significantly diminished for the southeastern region, despite the fact that, on average, the models are doing a somewhat better job of reproducing the ERBE spatial averages for the southeastern region relative to the western region (Figure 5). This underscores the point made in the Introduction, and by *Webb et al.* [2001], that comparisons involving solely regionally averaged TOA CRF can be misleading if there are compensating errors in cloud vertical structure or cloud optical depth.

[16] MPI and COLA serve to make the above point. Both produce minimal biases in Figure 5b, but they differ considerably from ERBE in the scatterplots of Figure 7. MPI to a lesser extent, and COLA to a greater extent, show a bifurcation suggestive of the models producing two distinctly different cloud types within the southeastern region. For COLA the horizontal branch could be associated with the presence of abnormally high clouds having variable cloud fraction over the region. Recall that horizontal scatter would be indicative of spatial variability of cloud fraction. Conversely, the vertical branch is probably suggestive of the presence of abnormally low clouds, since vertical scatter is indicative of variability in cloud-top height, and the vertical branch moves above the ERBE points, suggestive of the model producing abnormally low clouds in the upper portion of this branch. However, in the context of spatial averages, COLA produces very realistic results (Figure 5b), evidently as the result of compensating errors in cloud vertical structure and cloud fraction. Of the eight models in Figure 7, CCCMA produces the least amount of scatter, and the displacement of the model's points to the left of the ERBE points suggests that CCCMA is overestimating cloud fraction within the southeastern region. If so, it should likewise overestimate SW cooling, consistent with the large negative bias of SW CRF illustrated in Figure 5b. BMRC and NCAR are both noteworthy, since for the southeastern region they show considerable departures from the ERBE points (Figure 7), whereas for the western region they were two of the better models (Figure 6).

[17] The optical depths, fractions and altitudes of a GCM"s clouds can all contribute to errors in the model's CRF. Also, since CRF is referenced to the TOA clear-sky fluxes, then these clear-sky fluxes are also potential error sources for CRF. For this reason, we have compared clear-sky fluxes for 18 of the models (GISS did not supply clear fluxes) to those measured by ERBE. Biases, relative to ERBE, in the clear-sky SW reflection are summarized in Figure 8a. That NCAR has minimal biases is consistent with several studies which have compared that model's SW column radiation code to both surface and satellite radiometric measurements [e.g., *Waliser et al.*, 1996; *Jing and Cess*, 1998]. For several of the models, however, the biases are disturbingly large. Similar comparisons are summarized in Figure 8b for the clear-sky outgoing LW radiation (OLR), and here the situation is somewhat more complicated than in Figure 8a. This is because the clear-sky OLR depends not only on a model's LW radiation code, but also upon the vertical temperature and humidity profiles that a model produces. For example, it has been suggested (S. A. Klein, private communication, 2003) that the negative OLR bias for GFDL is consistent with that model having a cold bias in the tropical free troposphere plus excessive upper tropo-

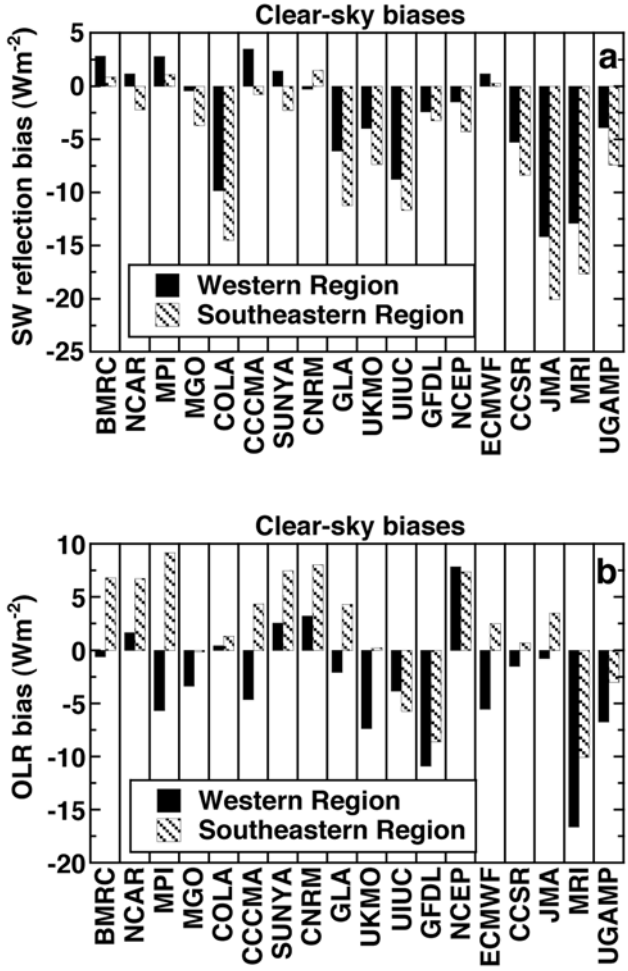

Figure 8. (a) Biases in the TOA reflected SW radiation for clear skies, relative to ERBE, for 18 GCMs. (b) The same as (a) but for the clear-sky OLR.

spheric humidity. On the other hand, for NCAR the modest positive biases are consistent with comparisons of that model's LW column radiation code with observed clear-sky OLR, for which observed temperature and humidity profiles were used as input to the column model [*Zhou and Cess*, 2000]. As with the SW biases, there are some substantial OLR biases shown in Figure 8b. It should be emphasized that the ERBE clear-sky OLR is based strictly on clear-sky sampling. GCMs, on the other hand, compute the clear-sky OLR by setting cloud fraction to zero in a second call to the radiation code. Thus the GCM clear-sky OLR refers to a more moist atmosphere than would be the case for true clear-sky sampling, and this by itself would contribute to a negative OLR bias [*Zhang et al.*, 1994]. This could thus explain the modest negative OLR biases that some models exhibit in Figure 8b.

4. Summary and Discussion

[18] We again emphasize that for a model to reliably project the future climate, it must, at the very least, reproduce the present observed climate, and this study provides an additional means of using satellite radiometric data for this purpose. Since the availability of the ERBE radiometric data, there have been numerous comparisons of GCM output to either the ERBE TOA SW and LW fluxes, or to the ERBE SW and LW CRF. The emphasis of this study is that the ERBE data, by means of the N versus Net CRF scatterplots, can additionally be used to assess a GCMs ability to produce, for the present climate system, realistic cloud vertical structure and/or optical depth, in addition to TOA radiative fluxes and CRF. However, a surprising result, unrelated to the scatterplot analyses, is that many of the 19 models produce unusually large biases in Net CRF (Figure 4a) that are all of the same sign (negative).

[19] A subset of eight models was used in the scatterplot analyses. For the western region, characterized by high clouds spanning the range from thin cirrus to deep convective clouds, seven of the models produced N versus Net CRF slopes that were reasonably representative of the slope determined from the ERBE data. However, the scatterplot analyses additionally revealed that two of these models (BMRC, NCAR) produced excessive thin cirrus, while four models (CCCMA, CNRM, COLA, GLA) produced a large percentage of clouds that were overly bright. The results for the southeastern region, characterized by trade cumulus, were the most revealing. If one only considered regional averages, the results summarized in Figure 5 would suggest that most models were in somewhat more realistic agreement with ERBE for this region than for the western region. However, the scatterplot analyses (Figures 6 and 7) show just the opposite, again emphasizing that spatially averaged CRF can be misleading because of compensating errors in cloud vertical structure or cloud optical depth. This underscores the utility of the scatterplot analysis, although it does have limitations. For example, it cannot be applied to regions containing stratocumulus clouds, because these low warm clouds produce very small LW CRF, and thus N would be large and highly variable.

[20] **Acknowledgments.** We thank two anonymous reviewers for their constructive comments and Dr. Wuyin Lin for providing us with the ISCCP data. This research was performed under the auspices of the U.S. Department of Energy (DOE) Office of Science, Biological and Environmental Research by the Lawrence Livermore National Laboratory under contract W-7405-ENG-48, and by the State University of New York at Stony Brook by the CERES Project through NASA contract NAS1-981421 and by the DOE Office of Science, Biological and Environmental Research through grants DEFG0290ER61063 and DEFG028ER6013.

References

Cess, R. D., et al. (1997), Comparison of the seasonal change in cloud-radiative forcing from atmospheric general circulation models and satellite observations, *J. Geophys. Res.*, *102*, 16,593–16,603.

Cess, R. D., M. H. Zhang, B. A. Wielicki, D. F. Young, X. L. Zhou, and Y. Nikitenko (2001a), The influence of the 1998 El Niño upon cloud-radiative forcing over the Pacific warm pool, *J. Clim.*, *14*, 2129–2137.

Cess, R. D., M. H. Zhang, P.-H. Wang, and B. A. Wielicki (2001b), Cloud structure anomalies over the tropical Pacific during the 1997/98 El Niño, *Geophys. Res. Lett.*, *28*, 4547–4550.

Gates, W. L., et al. (1999), An overview of the results of the Atmospheric Model Intercomparison Project (AMIP I), *Bull. Am. Meteorol. Soc.*, *80*, 29–56.

Hack, J. J. (1998), Sensitivity of the simulated climate to a diagnostic formulation for cloud liquid water, *J. Clim.*, *11*, 1497–1515.

Harrison, E. F., P. Minnis, B. R. Barkstrom, V. Ramanathan, R. D. Cess, and G. G. Gibson (1990), Seasonal variation of cloud radiative forcing derived from the Earth Radiation Budget Experiment, *J. Geophys. Res.*, *95*, 18,687–18,703.

Hartmann, D. L., L. A. Moy, and Q. Fu (2001), Tropical convection and the energy balance at the top of the atmosphere, *J. Clim.*, *14*, 4495–4511.

Jing, X., and R. D. Cess (1998), Comparison of atmospheric clear-sky shortwave radiation models to collocated satellite and surface measurements in Canada, *J. Geophys. Res.*, *103*, 28,817–28,824.

Kiehl, J. T. (1994), On the observed near cancellation between longwave and shortwave cloud forcing in tropical regions, *J. Climate*, *7*, 559–565.

Kiehl, J. T., and V. Ramanathan (1990), Comparison of cloud forcing derived from Earth Radiation Budget Experiment with that simulated by the NCAR Community climate Model, *J. Geophys. Res.*, *95*, 1,679–1,698.

Nemesure, S., R. D. Cess, E. G. Dutton, J. J. DeLuisi, Z. Li, and H. G. Leighton (1994), Impact of clouds on the shortwave radiation budget of the surface-atmosphere system for snow-covered surfaces, *J. Clim.*, *4*, 579–585.

Ramanathan, V., R. D. Cess, E. F. Harrison, P. Minnis, B. R. Barkstrom, E. Ahmad, and D. Hartmann (1989), Cloud-radiative forcing and climate: Results from the Earth Radiation Budget Experiment, *Science*, *243*, 57–63.

Rossow, W. B., and R. A. Schiffer (1991), ISCCP cloud data products, *Bull. Am. Meteorol. Soc.*, *72*, 2–20.

Waliser, D. E., W. D. Collins, and S. P. Anderson (1996), An estimate of the surface shortwave cloud forcing over the western Pacific during TOGA COARE, *Geophys. Res. Lett.*, *23*, 519–522.

Webb, M., C. Senior, S. Bony, and J.-J. Morctrette (2001), Combining ERBE and ISCCP data to assess clouds in the Hadley Centre, ECMWF and LMD atmospheric climate models, *Clim. Dyn.*, *17*, 905–922.

Zhang, M. H., R. D. Cess, T. Y. Kwon, and M. H. Chen (1994), Approaches of comparison for clear-sky radiative fluxes from general circulation models with Earth Radiation Budget Experimnet data, *J. Geophys. Res.*, *99*, 5515–5523.

Zhou, Y. P., and R. D. Cess (2000), Validation of longwave atmospheric radiation models using Atmospheric Radiation Measurements data, *J. Geophys. Res.*, *105*, 29,703–29,716.

Zhou, Y. P., and R. D. Cess (2001), Algorithm development strategies for retrieving the downwelling longwave flux at the Earth's surface, *J. Geophys. Res.*, 12,477–12,488.

R. D. Cess, Marine Sciences Research Center, State University of New York at Stony Brook, Stony Brook, NY 11790, USA. (rcess@notes.cc.sunysb.edu)

G. L. Potter, Program for Climate Model Diagnosis and Intercomparison, Lawrence Livermore National Laboratory, Livermore, CA 94550, USA. (gpotter@llnl.gov)